

# A NOVEL VISION-BASED REACTIVE NAVIGATION STRATEGY BASED ON INVERSE PERSPECTIVE TRANSFORMATION\*

Francisco Bonin-Font, Alberto Ortiz and Gabriel Oliver  
Department of Mathematics and Computer Science, University of the Balearic Islands  
Ctra de Valldemossa Km 7.5, 07122, Palma de Mallorca, Spain

Keywords: Mobile robots, Vision, Obstacle Avoidance, Feature Tracking, Inverse Perspective Transformation, SIFT.

Abstract: This paper describes a new vision-based reactive navigation strategy addressed to mobile robots, comprising obstacle detection and avoidance. Most of the reactive vision-based systems base their strength uniquely on the computation and analysis of quantitative information. The proposed algorithm combines a quantitative process with a set of qualitative rules to converge in a robust technique to safely explore unknown environments. The process includes a feature detector/tracker, a new feature classifier based on the Inverse Perspective Transformation which discriminates between object and floor points, and a qualitative method to determine the obstacle contour, their location in the image, and the course that the robot must take. The new strategy has been implemented on mobile robots with a single camera showing promising results.

## 1 INTRODUCTION

Visual techniques for detecting and tracking main scene features have been notably improved over the last few years and applied to robot navigation solutions. Zhou and Li (Zhou and Li, 2006) detected ground features grouping all coplanar points that have been found with the Harris corner detector (Harris and Stephens, 1988). Lowe (Lowe, 2004) developed the Scale Invariant Feature Transform (SIFT) method to extract highly discriminative image features, robust to scaling, rotation, camera view-point changes and illumination changes. Rodrigo *et al* (Rodrigo *et al.*, 2006) estimated the motion of a whole scene computing a homography matrix for every different scene plane. Mikolajczyk and Schmid (Mikolajczyk and Schmid, 2005) compared the performance of different descriptors for image local regions showing that, for different region matching approaches SIFT yields the best performance in all tests. The Inverse Perspective Transformation (*IPT*) has been successfully used in obstacle detection procedures. Mallot *et al* (Mallot *et al.*, 1991) analyzed variations on the optical flow computed over the Inverse Perspective Transformation of consecutive frames to detect the presence of obstacles. Bertozzi and Broggi (Bertozzi and

Broggi, 1997) applied the *IPT* to project two stereo images onto the ground. The subtraction of both projections generate a non-zero pixel zone that evidences the presence of obstacles. Ma *et al* (Ma *et al.*, 2007) presented an automatic pedestrian detector based on *IPT* for self guided vehicles. The system predicts new frames assuming that all image points lie on the floor, generating distorted zones that correspond to obstacles.

This paper addresses the problem of obstacle detection and avoidance for a safe navigation in unexplored environments. First, image main features are detected, tracked across consecutive frames, and classified as obstacles or ground using a new algorithm based on *IPT*. Next, the edge map of the processed frame is computed, and edges comprising obstacle points are discriminated from the rest of the edges. This result gives a qualitative idea about the position of obstacles and free space. Finally, a new version of the Vector Field Histogram (Borenstein and Koren, 1991) method, here adapted to systems equipped with visual sensors, is applied to compute a steering vector which points towards the areas into which the vehicle can safely move. The rest of the paper is organized as follows: the method is outlined in Section 2, experimental results are exposed and discussed in Section 3, and finally, conclusions and forthcoming work are given in Section 4.

\*This work is partially supported by DPI 2008-06548-C03-02 and FEDER funding.

## 2 THE NEW METHOD

### 2.1 Inverse Perspective Transformation

The Direct Perspective Transformation is the first-order approximation to the process of taking a picture. The line that connects a world point with the lens intersects the image plane and defines its unique image point. The Inverse Perspective Transformation specifies the straight line upon which the world point corresponding to a certain image point must lie. (Hartley and Zisserman, 2003) describes the Direct and Inverse Perspective Transformation processes and both are also modeled in (Duda and Hart, 1973), as well as the expressions to calculate the world coordinates for points lying on the floor ( $z = 0$ ):

$$x = X_0 - \frac{Z_0 x_p \cos \theta + (y_p \sin \varphi - f \cos \varphi)(Z_0 \sin \theta)}{y_p \cos \varphi + f \sin \varphi} \quad (1)$$

$$y = Y_0 - \frac{Z_0 x_p \sin \theta - (y_p \sin \varphi - f \cos \varphi)(Z_0 \cos \theta)}{y_p \cos \varphi + f \sin \varphi} \quad (2)$$

where  $(x_p, y_p)$  are the point image coordinates,  $(x, y)$  are the point world coordinates,  $(X_0, Y_0, Z_0)$  are the lens world coordinates at the moment in which the frame has been taken,  $f$  is the focal length, and  $\theta$  and  $\varphi$  are the yaw and pitch angles of the camera, respectively.

### 2.2 Obstacle and Ground Points

Presuming that all image points lie on the floor (i.e.  $z = 0$ ), their  $(x, y)$  world coordinates can be calculated using (1) and (2). This is an incorrect assumption for points of obstacles that protrude vertically from the floor. As a consequence, the  $(x, y)$  world coordinates (for  $z = 0$ ) of an obstacle point are different when they are calculated from two consecutive images, and different to the obstacle point real  $(x, y)$  world coordinates. However, the  $(x, y)$  world coordinates (for  $z = 0$ ) of a ground point, are equal when they are computed from two consecutive images, and equal to the real  $(x, y)$  ground point world coordinates. Hence, assuming  $z = 0$  and analyzing the distance between the resulting  $(x, y)$  point world coordinates for  $z = 0$ , calculated across two consecutive images, one can distinguish if the point belongs to an object or to the floor:

$$D = \sqrt{(x_2 - x_1)^2 + (y_2 - y_1)^2} \Rightarrow \begin{cases} \text{if } D > \beta \Rightarrow \text{obstacle,} \\ \text{if } D \leq \beta \Rightarrow \text{ground.} \end{cases} \quad (3)$$

where  $(x_1, y_1)$  and  $(x_2, y_2)$  are the  $(x, y)$  feature world coordinates (for  $z = 0$ ) at instants  $t_1$  and  $t_2$  respectively

and  $\beta$  is the threshold for the maximum difference admissible between  $(x_1, y_1)$  and  $(x_2, y_2)$  to consider both as the same point. Ideally  $\beta$  should be 0.

Figure 1 illustrates the idea. Two frames of a scene are taken at instants  $t_1$  and  $t_2$ . Point  $P_{2w}$  is on the ground. Its projection into the image plane at instants  $t_1$  and  $t_2$  generates, respectively, the image points  $P_{2i0}$  and  $P_{2i1}$ . The Inverse Transformation of  $P_{2i0}$  and  $P_{2i1}$  generates a single point  $P_{2w}$ .  $P_{1w}$  is an obstacle point. Its projection into the image plane at  $t_1$  and  $t_2$  generates, respectively, points  $P_{1i0}$  and  $P_{1i1}$ . However, the projection of  $P_{1i0}$  and  $P_{1i1}$  onto the ground plane (i.e. Inverse Transformation assuming  $z = 0$ ) generates two different points on the ground, namely,  $P'_{1w}$  and  $P''_{1w}$ .

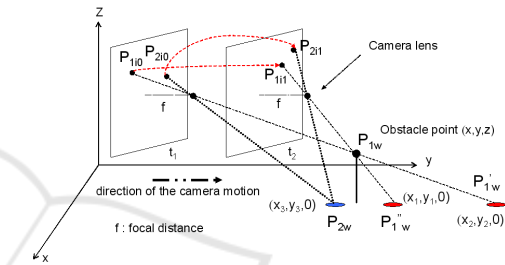


Figure 1: The IPM-based obstacle detection principle.

### 2.3 Feature Detection and Tracking

The first step of the obstacle detection algorithm is to find a sufficiently large and relevant set of image points, and establish a correspondence of all these points between consecutive frames. SIFT features (Lowe, 2004) have been chosen as the features to track because of their robustness to scale changes, rotation and/or translation as well as changes in illumination and view point. In order to filter out possible wrong correspondences between points in consecutive frames, outliers are filtered out using RANSAC and imposing the epipolar constraint. After the detection and tracking process, features are classified as ground or obstacle.

Small changes in the distance threshold  $\beta$  can alter the classification of those points which have a  $D$  value (3) close to  $\beta$ . In order to decrease the sensitivity of the classifier with regard to  $\beta$ , all these points are left unclassified. Additionally, in a previous training phase, and for each different scene, histograms of  $D$  values for well classified and misclassified points are built and analyzed. For every different scene,  $D$  values of ground points wrongly classified as obstacle are stored in a database. In the autonomous navigation phase, all object points with a  $D$  value included in that set of stored  $D$  values of the current scene, are neither

classified. In this way, nearly all ground points classified as obstacles are eliminated, reducing the risk of detecting false obstacles, and although some true obstacle points are also removed, the remaining ones are sufficient to permit the detection of those obstacles.

## 2.4 Obstacle Profiles and the Navigation Strategy

SIFT features are usually detected at regions of high intensity variation (Lowe, 2004) and besides, commonly they are near or belong to an edge. Obstacles usually have a high degree of vertical edges and have one or some points in contact with the floor. All detected obstacle points are most likely to be contained or near a vertical edge which must belong to that obstacle. Hence, the next step of the algorithm is the computation of the processed images edge map, and the detection of all complete edges that comprise real obstacle points. This permits to isolate the obstacle boundaries from the rest of the edges and to get a qualitative perception of the environment. Obstacle points wrongly classified as ground can be reclassified if they are comprised in an edge that contains other obstacle points.

In order to combine a high degree of performance in the edge map computation with a relatively low processing time, our edge detection procedure runs in two steps (Canny, 1986): a) The original image is convolved with a 1D gaussian derivative, detecting zones with high vertical gradient from smoothed intensity values with a single convolution; b) A process of hysteresis thresholding is applied. Two thresholds are defined. A pixel with a gray level above the highest threshold is classified as edge pixel. A pixel with a gray level above the lowest threshold is classified as edge if it has in its vicinity a pixel with a gray value higher than the highest threshold.

The proposed navigation strategy has been inspired by (Borenstein and Koren, 1991). Only obstacles detected inside a *ROI* (Region of Interest) centered at the bottom of the image are considered to be avoided. This guarantees a virtual 3-D sphere of safety around the robot. The image *ROI* is in turn divided in angular regions. Those polar directions, corresponding to angular regions occupied by a real obstacle boundary are labeled as forbidden and those free of obstacle boundaries are included in the set of possible next movement directions. This process results in a polar map of free and occupied zones. Obstacle-free polar regions which are narrower than a certain threshold (determined empirically and depending on the robot size) are excluded from the possible motion directions. If all angular regions are

narrower than the defined threshold, the algorithm returns a stop order. The next movement direction is given as a vector, pointing to the widest polar obstacle-free zone. Positive angles result for turns to the right and negative angles for turns to the left. The computed steering vector qualitatively points towards the free space and the complete algorithm gives a reasonable idea of whether this free space is wide enough to continue the navigation through it.

## 3 EXPERIMENTAL RESULTS

A Pioneer 3Dx mobile robot with a calibrated wide angle camera was programmed to navigate at 40mm/s in different environments to test the proposed strategy: environments with obstacles of regular and unregular shape, environments with textured and untextured floor, and environments with specularities or with low illumination conditions. Operative parameter settings: image *ROI* = 85 pixels; for the hysteresis thresholding: low level= 40 and high levels= 50; camera height= 430mm;  $\varphi = -9^\circ$ ; initial  $\theta = -2^\circ$ , and finally,  $f = 3.720mm$ . For each scene, the complete navigation algorithm was run over successive pairs of 0.56-second-separation consecutive frames so that the effect of *IPT* was noticeable. Increasing the frame rate decreases the *IPT* effect over the obstacle points, and decreasing the frame rate delays the execution of the algorithm. Frames were recorded and down-sampled to a resolution of  $256 \times 192$  pixels, in order to reduce the computation time. All frames were also undistorted to correct the error in the image feature position due to the distortion introduced by the lens, and thus, to increase the accuracy in the calculation of the point world coordinates.

In order to assess the classifier performance ROC curves were computed, defining obstacle points classified as obstacle as true positives (*TP*), obstacle points classified as ground as false negatives (*FN*), ground points classified as floor as true negatives (*TN*) and ground points classified as obstacles as false positives (*FP*). The AUC (Area Under the Curve) were calculated as a measure of success classification rate, suggesting success rates greater than 93% (Bonin-Font et al., 2008). The  $\beta$  operational value (3) was obtained for every scene minimizing the cost function  $f(\beta) = FP(\beta) + \lambda FN(\beta)$ . During the experiments,  $\lambda$  was set to 0.5 to prioritize the minimization of false positives over false negatives. The value of  $f(\beta)$  was calculated for every pair of successive images, changing  $\beta$ . For a varied set of scenes differing in light conditions and/or floor texture, the optimum  $\beta$  had a coincident value of 20mm.

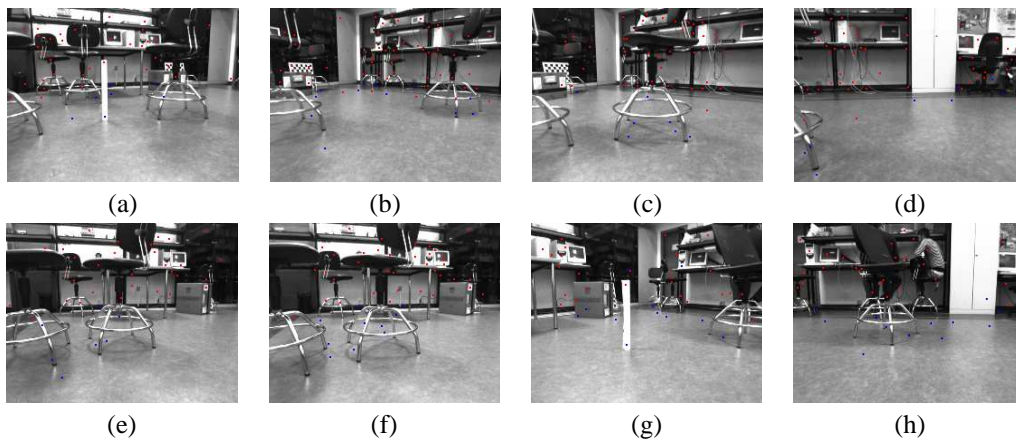


Figure 2: Scene 1. (a) to (d)- Experiment 1. (e) to (h)- Experiment 2: Object and floor points after the filter.

Images (a), (b), (c) and (d) of figure 2 show the undistorted second frame of several pairs of consecutive images, recorded and processed on-line. Images show SIFT features classified as ground (blue) and classified as obstacles (red). Every image was taken just before the robot had to turn to avoid the obstacles it had in front. Notice that all four pictures present a few false positives on the floor.

Histograms of  $D$  values for  $TP$  (in blue) and  $FP$  (in red) are presented in figure 3. Plot (a) corresponds to scene 1 (figure 2), plot (b) to scene 2, plot (c) to scene 3 and plot (d) corresponds to scene 4. Scenes 2,3 and 4 are shown in figure 4. These histograms count false and true positives for different  $D$  values, in all frames recorded and computed by the algorithm during a complete sequence. Although histograms belong to environments with different lighting conditions or floor textures, and scenarios with inter-reflections or specularities, results were commonly similar: most of the true positives presented  $D$  values between 20mm and 300mm, and the majority of false positives had  $D$  values between 20mm and approximately 80mm. All positives with  $D$  values between 20mm and 80mm were filtered and left unclassified. This filtering process increases AUCs until the 96%, however, obstacle points near the floor have more probabilities of been miss-classified than others since their  $D$  value can be lower than 20mm.

Pictures (e) to (h) of figure 2 were taken during a second experiment through the environment of scene 1. In this experiment, the filter outlined in the previous paragraph was applied. Notice that all false positives have been eliminated. This reduces the risk of detecting false obstacles but maintains a sufficient number of true positives to detect the real obstacles. After the process of feature detection, tracking, and classification, the algorithm localizes every ob-

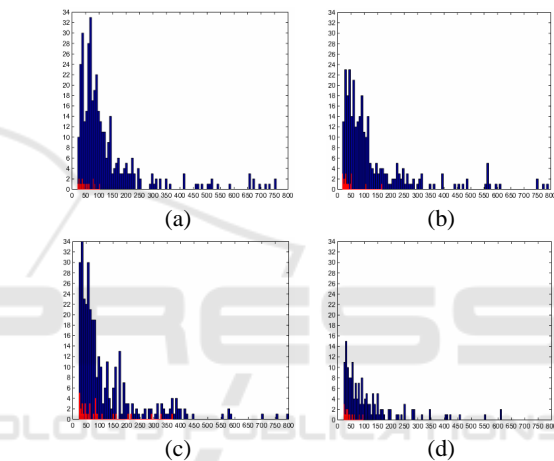


Figure 3: Histograms of  $D$  values:  $TP$  (blue) and  $FP$  (red).

ject point in the edge map of the second frame, and then searches for all edge pixels which are inside a patch window of  $8 \times 13$  pixels, centered in the feature image coordinates. Every edge is tracked down starting from the object point position until the last edge pixel is found, and considering this last edge pixel to be the point where the object rests on the floor. This process results into the identification of the object vertical contours. The consecutive execution of the complete algorithm using successive image pairs as input results in a collection of consecutive steering vectors used as the continuous motion orders. After every robot turn, the value of the camera yaw angle is updated, adding the turn angle to the previous yaw value. The camera world coordinates are calculated composing the robot orientation and its center world coordinates obtained via dead reckoning, with the relative camera position respect to the center of the robot.

Pictures from (a) to (d), (i) to (l) and (p) to (s) in figure 4 show the second frame of different pairs



of consecutive images, recorded and processed during the navigation through the scenarios 2, 3 and 4, respectively. Every image was taken before the robot had to turn to avoid the frontal obstacles, and show obstacle (in red) and ground points (in blue). Scene 2 presents inter-reflections, specularities, and a lot of obstacles with regular and irregular shapes. Scene 3 shows a route through a corridor with a very high textured floor, columns and walls. Scene 4 presents bad illumination conditions, a lot of inter-reflections on the floor, and some image regions (walls) with almost homogeneous intensities and/or textures, which results in few distinctive features and poorly edged obstacles. Walls with a very homogeneous texture and few distinctive features can present difficulties for its detection as an obstacle. In all scenes, all obstacle points with a  $D$  value between 20mm and 80mm were left unclassified, except in scene 4, where, only those obstacle points with a  $D$  value between 20mm and 45mm were filtered out. Pictures (e) to (h), (z) to (o) and (t) to (x) of figure 4 show the vertical contours (in orange) comprising obstacle points. See attached to every picture the angle of the computed steering vector. For example, in picture (x) objects are out of the  $ROI$ , then, the computed turn angle is  $0^\circ$  (follow ahead). In picture (e) the obstacles are partially inside the  $ROI$ , so the robot turns to the right ( $40^\circ$ ). Despite scene 4 presents a poor edge map and few SIFT features, the resulting steering vectors still guide the robot to the obstacles-free zone. Plots (1) to (4) show an illustration of the environment and the robot trajectory (blue circle: the starting point; red circle: the final point) for scenes 1, 2, 3 and 4, respectively. In all scenes, all features were well classified, obstacle profiles were correctly detected and the robot navigated through the free space avoiding all obstacles. The steering vector is computed on the image and then it is used qualitatively to guide the robot.

## 4 CONCLUSIONS

This paper introduces a new vision-based reactive navigation strategy addressed to mobile robots. It employs an  $IPT$ -based feature classifier that distinguishes between ground and obstacle points with a success rate greater than 90%. The strategy was tested on a robot equipped with a wide angle camera and showed to tolerate scenes with shadows, inter-reflections, and different types of floor textures or light conditions. Experimental results obtained suggested a good performance, since the robot was able to navigate safely. In order to increase the classifier success rate, future research includes the evaluation

of the classifier sensitivity to the camera resolution or focal length. The use of various  $\beta$  values, depending on the image sector that  $D$  is being evaluated, can also increase the classifier performance.

## REFERENCES

- Bertozzi, M. and Broggi, A. (1997). Vision-based vehicle guidance. *Computer*, 30(7):49–55.
- Bonin-Font, F., Ortiz, A., and Oliver, G. (2008). A novel image feature classifier based on inverse perspective transformation. Technical report, University of the Balearic Islands. A-01-2008 (<http://dmi.uib.es/fbonin>).
- Borenstein, J. and Koren, I. (1991). The vector field histogram - fast obstacle avoidance for mobile robots. *Journal of Robotics and Automation*, 7(3):278–288.
- Canny, J. (1986). A computational approach to edge detection. *IEEE TPAMI*, 8(6):679 – 698.
- Duda, R. and Hart, P. (1973). *Pattern Classification and Scene Analysis*. John Wiley and Sons Publisher.
- Harris, C. and Stephens, M. (1988). Combined corner and edge detector. In *Proc. of the AVC*, pages 147–151.
- Hartley, R. and Zisserman, A. (2003). *Multiple view geometry in computer vision*. Cambridge University Press, ISBN: 0521623049.
- Lowe, D. (2004). Distinctive image features from scale-invariant keypoints. *International Journal of Computer Vision*, 60(2):91–110.
- Ma, G., Park, S., Mller-Schneiders, S., Ioffe, A., and Kummert, A. (2007). Vision-based pedestrian detection - reliable pedestrian candidate detection by combining ipm and a 1d profile. In *Proc. of the IEEE ITSC*, pages 137–142.
- Mallot, H., Buelthoff, H., Little, J., and Bohrer, S. (1991). Inverse perspective mapping simplifies optical flow computation and obstacle detection. *Biological Cybernetics*, 64(3):177–185.
- Mikolajczyk, K. and Schmid, C. (2005). A performance evaluation of local descriptors. *IEEE TPAMI*, 27(10):1615–1630.
- Rodrigo, R., Chen, Z., and Samarabandu, J. (2006). Feature motion for monocular robot navigation. In *Proc. of the ICIA*, pages 201–205.
- Zhou, J. and Li, B. (2006). Homography-based ground detection for a mobile robot platform using a single camera. In *Proc. of the IEEE ICRA*, pages 4100–4101.

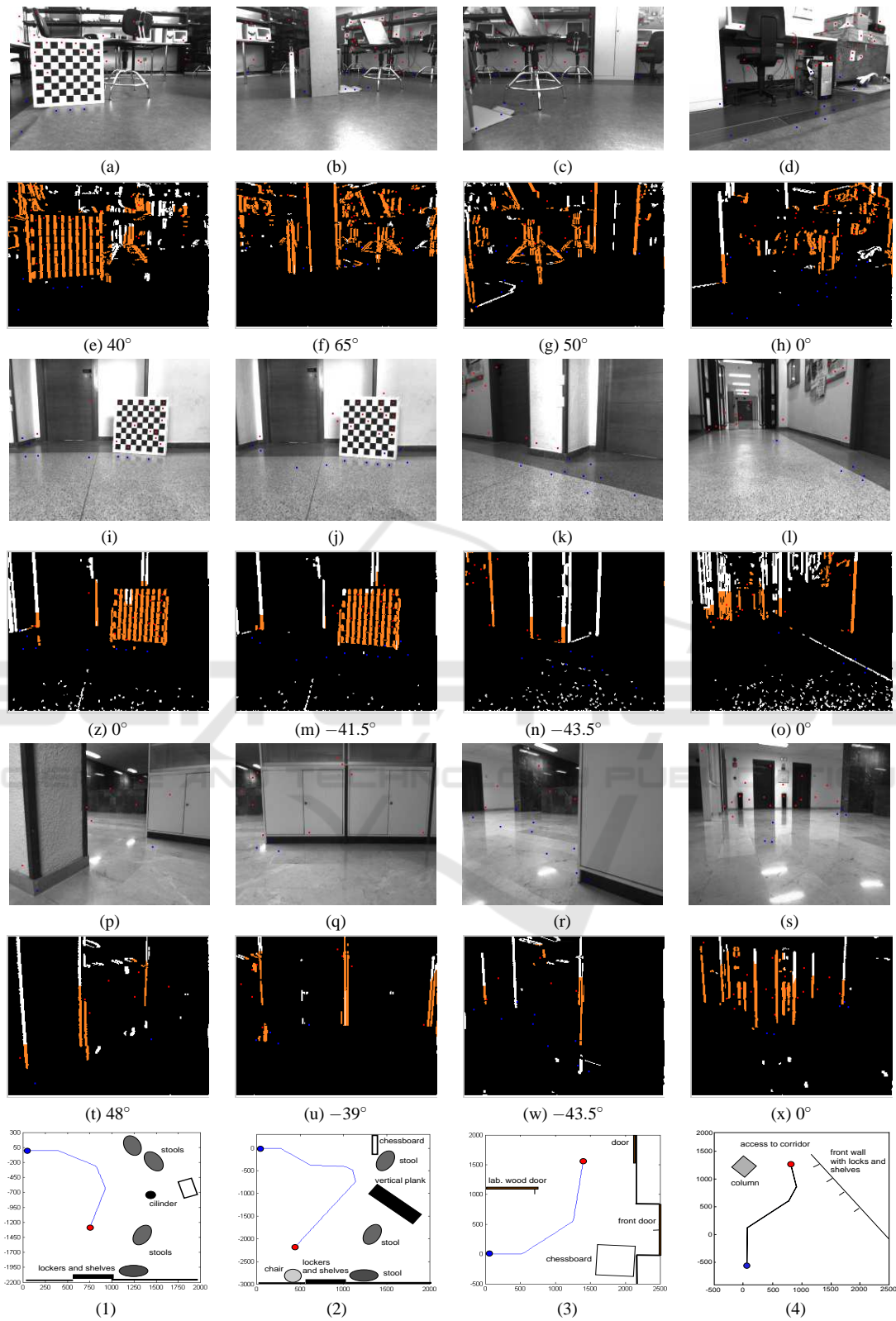


Figure 4: (a) to (d) Scene 2, (i) to (l) Scene 3, (p) to (s) Scene 4. (e) to (h), (z) to (o) and (t) to (x), vertical contours of Scene 2, 3 and 4, respectively. (1) to (4): robot trajectories.